to apply these results for developing new robust nonlinear control laws based on dynamic neural networks.

APPENDIX A

To prove inequality $X^T Y + Y^T X \leq X^T \Lambda X + Y^T \Lambda^{-1} Y$, $; X \in \Re^{n \times k}$, $Y \in \Re^{n \times k}$, $\Lambda \in \Re^{n \times n}$, it suffices to demonstrate that $F \equiv X^T \Lambda X + Y^T \Lambda^{-1} Y - X^T X - Y^T Y \geq 0$, $F \in \Re^{k \times k}$ or, equivalently, $\forall v \in \Re^k$, $v^T F v \geq 0$. Denoting $v_1 = \lambda^{1/2} X v$ and $v_2 = \Lambda^{-1/2} Y v$, then $v^T F v = v_1^T v_1 + v_2^T v_2 - 2 v_1^T v_2 = \| v_1 - v_2 \|^2 \geq 0$. This proof was first presented in [17].

APPENDIX B

1) Class K_∞ Function [2]: A continuous function $f \colon [0, a) \to [0, \infty)$ is said to belong to class K if it is strictly increasing and $f(0) = 0$ and it is said to belong to class K_∞ if $a = \infty$ and $\lim_{r \to \infty} f(r) = \infty$.

2) GAS [2]: Let $x = 0$ be an equilibrium point of $\dot{x} = f(x)$ and $D \subset \Re^n$ be a union of open connected set, with none of its boundary points, which contains $x = 0$. Let $V \colon D \to R$ be a continuously differentiable function such that $V(0) = 0$, $V(x) > 0$ and $\dot{V}(x) < 0$ in $D - \{0\}$, then $x = 0$ is asymptotically stable. If the property is fulfilled for $D = \Re^n$, then it is global.

3) ISS Lyapunov Function [12]: A function $V(x) \colon \Re^n \to \Re^+$ is defined as ISS Lyapunov if there exist $\alpha(\cdot)$, $\theta(\cdot)$ class K_∞ functions such that $\dot{V}(x) \leq -\alpha(\|x\|) + \theta(\|u\|)$, $\forall x \in \Re^n$, $\forall u \in \Re^m$.

ACKNOWLEDGMENT

REFERENCES

[1] A. N. Michel, J. A. Farrel, and W. Porod, "Qualitative analysis of neural networks," *IEEE Trans. Circuits Syst.,* vol. 36, pp. 229–243, Feb. 1989.
[2] H. K. Khalil, *Nonlinear Systems,* 2nd ed. Englewood Cliffs, NJ: Prentice-Hall, 1996.
[3] M. W. Hirsch, "Convergent activation dynamics in continuous time networks," *Neural Networks,* vol. 2, pp. 331–349, 1989.
[4] D. G. Kelly, "Stability in contractive nonlinear neural networks," *IEEE Trans. Biomed. Eng.,* vol. 3, pp. 241-242, Mar. 1990.
[5] K. Matsouka, "Stability conditions for nonliner continuous neural networks with asymmetric connections weights," *Neural Networks,* vol. 5, pp. 495–500, 1992.
[6] E. Kaszkurewics and A. Bhaya, "On a class of globally stable neural circuits," *IEEE Trans. Circuits Syst. I,* vol. 41, pp. 171–174, Feb. 1994.
[7] M. Forti *et al.,* "Necessary and sufficient conditions for absolute stability of neural networks," *IEEE Trans. Circuits Syst. I,* vol. 41, pp. 171–174, July 1994.
[8] P. P. Varaiya and R. Liu, "Bounded-input bounded output stability of nonlinear time-varying differential systems," *SIAM J. Contr.,* vol. 4, pp. 698–704, 1966.
[9] E. D. Sontag, "Smooth stabilization implies coprime factorization," *IEEE Trans. Automat. Contr.,* vol. 34, pp. 435–443, Apr. 1989.
[10] J. Tzinias, "Sontag's input to state stability condition and global stabilization using state detection," *Syst. Contr. Lett.,* vol. 20, pp. 219–226, 1993.
[11] Z. P. Jiang, A. Teel, and L. Praly, "Small-gain theorem for ISS systems and applications," *Math. Contr., Signals, Syst.,* vol. 7, pp. 104–130, 1994.
[12] E. D. Sontag, "On the input to state stability property," *Eur. J. Contr.,* vol. 1, pp. 1–24, 1995.
[13] E. N. Sanchez and J. P. Perez, "Input-to-state stability (ISS) analysis for dynamics neural networks," in *Proc. 1997 IEEE Int. Joint Conf. Neural Networks,* Houston, TX, June 1997, pp. 1139–1143.
[14] R. G. Bartle, *The Elements of Real Analysis,* 2nd ed. New York: Wiley, 1976.
[15] E. B. Kosmatopoulos, M. A. Christodoulou, and P. A. Ioannou, "Dynamical neural networks that ensure exponential identification error convergence," *Neural Networks,* vol. 10, pp. 299–314, 1997.
[16] M. Krstic and Z. H. Li, "Inverse optimal design of input to state stabilizing nonlinear controller," *IEEE Trans. Automat. Contr.,* vol. 43, pp. 316–350, Mar. 1998.
[17] A. S. Poznyak and E. N. Sanchez, "Nonlinear systems approximation by neural networks: Error stability analysis," *Intell. Automat. Soft Compt., Int. J.,* vol. 1, pp. 247–258, 1995.

Very Wide Range Tunable CMOS/Bipolar Current Mirrors with Voltage Clamped Input

Teresa Serrano-Gotarredona, Bernabé Linares-Barranco, and Andreas G. Andreou

Abstract—In low power current mode signal processing circuits it is often necessary to use current mirrors to replicate and amplify/attenuate current signals and clamp the voltage of nodes with high parasitic capacitances so that the smallest currents do not introduce unacceptable delays. The use of tunable active-input current mirrors would meet both requirements. In conventional active-input current mirrors, stability compensation is required. Furthermore, once stabilized, the input current cannot be made arbitrarily small. In this paper we introduce two new active-input current mirrors that clamp their input node to a given voltage. One of them does not require compensation, while the other may under some circumstances. However, for both, the input current may take any value. The mirrors can operate with their transistors biased in strong inversion, weak inversion, or even as CMOS compatible lateral bipolar devices. If it is biased in weak inversion or as lateral bipolars, the current mirror gain can be tuned over a very wide range. According to the experimental measurements provided in this paper, the input current may spawn beyond nine decades and the current mirror gain can be tuned over 11 decades. As an application example, a sinusoidal g_m-C-based VCO has been fabricated, whose oscillation frequency could be tuned for over seven decades, between 74 mHz and 1 MHz.

Index Terms—Analog VLSI circuits, BiCMOS circuits, current mirrors, current mode circuits, operational transconductance amplifiers, sinusoidal oscillators, stability compensation, tunable amplifiers.

I. INTRODUCTION

When using current mode signal processing VLSI circuits it is not unusual that a very wide range of current levels must be handled. For example, when building low-power silicon retinas, light intensity is directly and (approximately) linearly transformed into current [1], [2]. Silicon retinas can sense up to six decades of light levels, which also
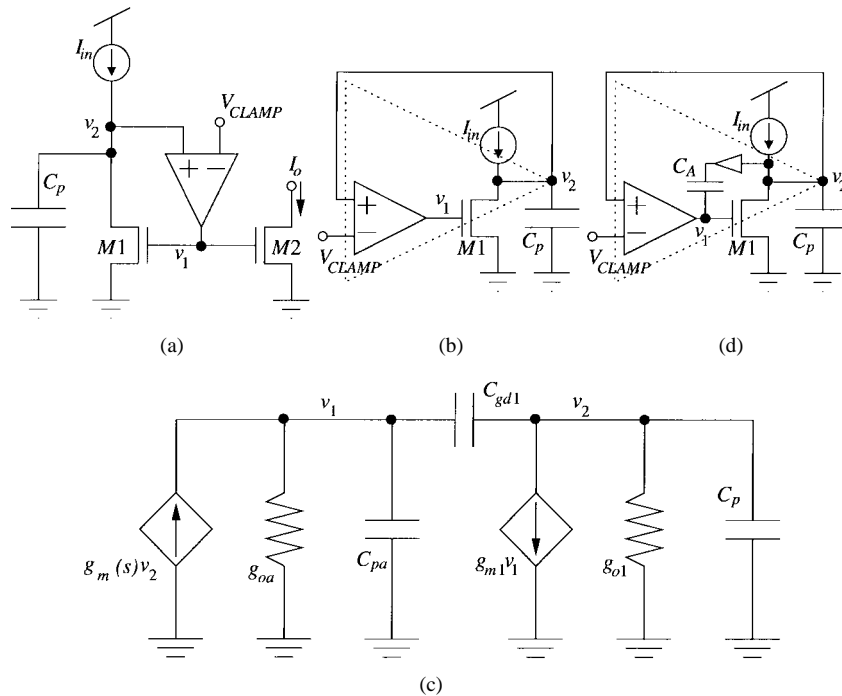
Fig. 1. Conventional active-input current mirror. (a) Circuit schematic representation. (b) Input stage drawn as a two-stage op amp. (c) Small-signal equivalent circuit for the mirror input stage. (d) Compensated circuit.

yields six decades of current levels at the photoreceptors' output. It is impractical to permit this current directly control the time constant of the complete system. This would make a silicon retina fast for high ambient light, but six orders of magnitude slower for low ambient light. This is not realistic and a way to lessen these delays is to clamp the voltages of those nodes with high parasitic capacitances. Since current mirrors are necessary elements for current mode signal processing circuits, a very compact solution is to use current mirrors that clamp their input voltages. These current mirrors are usually referred to as active-input current mirrors [3], [4].

In Section II, the conventional active-input current mirror is analyzed and it is shown why it needs compensation, why compensation depends on the mirror input current, and why this current cannot be made arbitrarily small. In Section III, two new source-driven active-input current mirror topologies are introduced and the stability is analyzed. One of the mirrors does not require compensation, while the other may require compensation under some circumstances. However, for both structures, the input current can be made arbitrarily small without creating unstable behavior. Section IV provides analysis for the dynamic behavior of the mirrors. Section V shows how to make the mirrors have a continuously adjustable gain, tunable over a very large range. Section VI studies loading effects. In Section VII, it is shown how to extend the mirroring operations to bipolar transistors, using CMOS compatible lateral bipolar transistors and, finally, in Section VII, experimental measurements are provided, which show the input currents spawning beyond six decades and the current mirror gains being adjusted over 11 decades. As an application example, the first mirror is used to make a constant linear input range OTA, whose transconductance is tunable for over seven decades. This OTA is then used in a g_m-C sinusoidal VCO, whose oscillating frequency could be tuned from 74 mHz to 1 MHz.

II. CONVENTIONAL ACTIVE INPUT CURRENT MIRROR

The conventional active-input current mirror [3] is shown in Fig. 1(a). By redrawing its input stage, as shown in Fig. 1(b), one recognizes a standard (uncompensated) two-stage CMOS operational amplifier (op amp) [5], connected in a unity-gain negative feedback configuration. The first stage of the op amp is the differential input amplifier of Fig. 1(a). The second (inverting) stage consists of transistor $M1$ and current source I_{in}. It is well known that this structure needs compensation [5] and that the compensation circuitry depends on the value of the second-stage bias current I_{in}. Furthermore, it results impractical to compensate when I_{in} reaches very low values.

For the differential input voltage amplifier, the OTA in Fig. 2(a) can be used. OTA's are compensated by their load capacitance C'_{pa}. An OTA connected in a unity gain feedback configuration [as in Fig. 2(b)] has the small-signal equivalent circuit shown in Fig. 2(c), where element $g_m(s)$ models the transconductance gain of the OTA and g_{oa} its output conductance. Transconductance $g_m(s)$ is frequency dependent because of the delay introduced by the parasitic capacitances of the OTA internal nodes. This delay can be modeled as [6]

$$g_m(s) = g_{ma}\left(1 - \frac{s}{\omega_a}\right) \qquad (1)$$

where g_{ma} is the dc transconductance gain of the OTA and ω_a models its delay. This yields the following stability condition for the circuit in Fig. 2(c):

$$C_{pa} > \frac{g_{ma}}{\omega_a}. \qquad (2)$$

Using this model for the OTA with the stability condition of (2), it is possible to analyze the stability for the circuit in Fig. 1(b), whose small-signal equivalent circuit is shown in Fig. 1(c). Transistor $M1$ is modeled by elements g_{m1}, g_{o1}, and C_{gd1}, while the OTA is modeled by $g_m(s) = g_{ma}(1 - s/\omega_a)$, g_{oa} and the node v_1 parasitic capacitance C_{pa}. After straightforward analysis it is easy to see that, if (2) is satisfied, imposing the condition

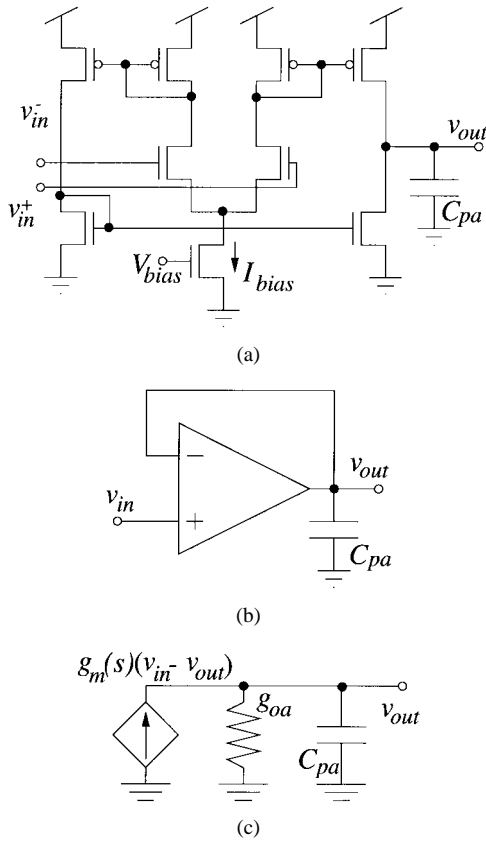$$C_{gd1}(g_{m1} - g_{ma}) > \frac{g_{m1}g_{ma}}{\omega_a} \qquad (3)$$

Fig. 2. (a) An OTA structure suitable for the differential input voltage amplifier. (b) Unity gain feedback configuration. (c) Small-signal equivalent circuit.

guarantees stability. However, this requires at least that $g_{m1} > g_{ma}$, which imposes a lower bound on the value of g_{m1} (and I_{in}) in Fig. 1(b). In practice, the circuit is usually compensated as shown in Fig. 1(d) [3], by adding a unity gain voltage buffer and a compensation capacitor C_A. Equation (3) would change to

$$g_{m1}(C_{gd1} + C_A) > \frac{g_{m1}g_{ma}}{\omega_a} + g_{ma}C_{gd1}. \tag{4}$$

However, again, g_{m1} cannot be made arbitrarily small.

The two new active-input current mirror topologies introduced in this paper do not have this problem; g_{m1} (and consequently, I_{in}) can be made arbitrarily small. In the next section these mirrors are introduced and analyzed.

III. Two New Active Input Current Mirrors

A. First Topology

The first alternative circuit to the one in Fig. 1(a) is shown in Fig. 3(a), where the OTA output drives the source of transistor $M1$ instead of its gate. The OTA must be able to sink twice the maximum expected value for I_{in}, which imposes an important design constraint for the OTA in that I_{bias} in Fig. 2(a) must be at least twice the maximum operation current of the mirror.[1] The mirror input stage can be redrawn, as shown in Fig. 3(b), which can be considered to be a special two-stage op amp, connected in a unity gain feedback configuration. Note that the second stage of this op amp is a positive-gain voltage amplifier, as opposed to the case of Fig. 1(b). Neglecting the body effect of transistor $M1$, the absolute

[1] Eventually, special OTA's that operate in a type of class AB mode [7] could be used to optimize power consumption.

gain value of this second stage would be identical to that of Fig. 1(b). Also note that the input node of this second stage is the source of transistor $M1$, which is a low-impedance node. This makes the circuit of Fig. 1(b) have a single dominant pole and, consequently, its behavior is qualitatively similar to a single-stage op amp in a unity gain feedback configuration. To analyze the stability conditions for this circuit, let us refer to its small-signal equivalent circuit, shown in Fig. 3(c). Its characteristic equation is

$$as^2 + bs + c = 0$$
$$\begin{cases} a = C_p C_{pa} \\ b = (g_{oa} + g_{m1})C_p - \dfrac{g_{m1}g_{ma}}{\omega_a} + g_{o1}\left(C_{pa} - \dfrac{g_{ma}}{\omega_a}\right) \\ c = g_{m1}g_{ma}. \end{cases} \tag{5}$$

Since the OTA is assumed to be compensated, (2) is satisfied and the last term for coefficient b in (5) is positive. However, b might still become negative. The following condition guarantees a positive b coefficient

$$C_p > \frac{g_{ma}g_{m1}}{\omega_a(g_{oa} + g_{m1})}. \tag{6}$$

This can be achieved by either adding an extra capacitance at node v_2 or by making the OTA have a smaller delay (larger ω_a) or lower g_{ma}. Note that the right-hand side of (6) is an increasing function of g_{m1}. Consequently, once (6) is satisfied for the maximum possible g_{m1} (maximum I_{in}) stability is guaranteed for any smaller value of g_{m1} (and I_{in}).

If (6) cannot be satisfied, another way to achieve compensation for this topology is by adding a compensation capacitor C_A between nodes v_1 and v_2 in Fig. 3. This yields the following characteristic equation:

$$as^2 + bs + c = 0$$
$$\begin{cases} a = C_p C_{pa} + C_A\left(C_p + C_{pa} - \dfrac{g_{ma}}{\omega_a}\right) \\ b = C_p(g_{oa} + g_{m1}) + g_{o1}\left(C_{pa} - \dfrac{g_{ma}}{\omega_a}\right) + g_{ma}\left(C_A - \dfrac{g_{m1}}{\omega_a}\right) \\ c = g_{m1}g_{ma}. \end{cases}$$
$$\tag{7}$$

If (2) is satisfied, coefficient a is positive, as well as the second term of coefficient b. Consequently, stability is guaranteed if

$$C_A > g_{m1}\left(\frac{1}{\omega_a} - \frac{C_p}{g_{ma}}\right) - C_p \frac{g_{oa}}{g_{ma}}. \tag{8}$$

If the right-hand side of (8) is negative, C_A is not necessary and (6) results. If the right-hand side of (8) is positive, then C_A should satisfy (8) for the largest value of g_{m1} (or I_{in}). Once this is assured, (8) remains valid for any smaller value of g_{m1} (or I_{in}).

B. Second Topology

Another alternative active-input current mirror is the one shown in Fig. 3(d). Note that in this case transistor $M1$ is connected as a diode around the negative feedback loop of the amplifier and acts simply as a passive device. Therefore, if the differential voltage amplifier is already compensated for unity gain feedback, the circuit should always be stable. This can be verified by performing a similar analysis to that for the first topology.

C. Discussion

The stability analyses for both topologies are valid whether transistors $M1$ and $M2$ are biased in their weak or strong inversion regions of operation. This allows the current mirrors to operate for a very wide range of currents, from values equal to junction leakage
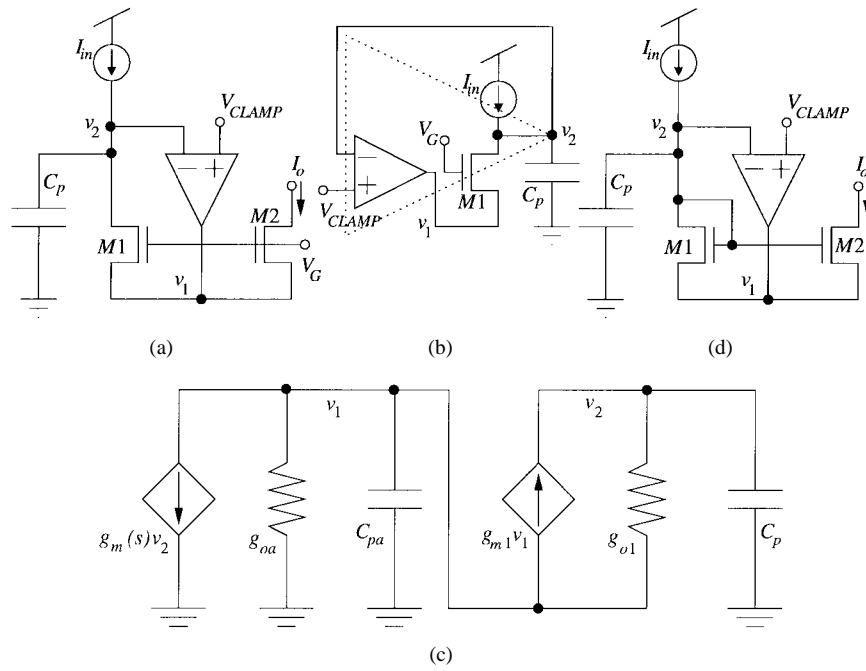
Fig. 3.   First new active-input current mirror topology. (a) Circuit schematic representation. (b) Input stage drawn as a two-stage op amp. (c) Small-signal equivalent circuit. (d) Second current mirror topology.
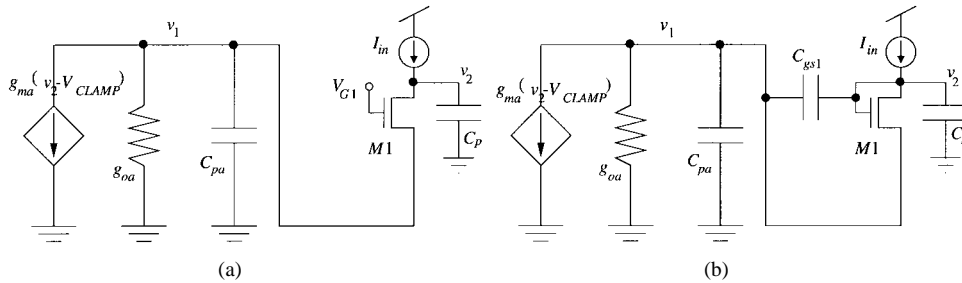

Fig. 4.   Equivalent circuits for computing transient analysis if OTA delay cannot be neglected. (a) The first new topology. (b) The second new topology.

currents, up to the maximum current the OTA might be able to sink. In addition, one must avoid having the OTA output voltage reach its minimum (or maximum, for p-type current mirrors) value, by adjusting V_{CLAMP} to a safe level.

The stability advantages for these two new topologies, with respect to the conventional one of Section II, come from the fact that the differential voltage amplifier is loaded by a low-impedance node, which makes the whole circuit to behave similarly to a single-pole (or one-dominant-pole) system. Although the Topology 1 current mirror might require stability compensation, it has certain advantages over the Topology 2 one, as will be seen throughout the paper. It is faster for very low currents and it can be operated in bipolar mode by simply rebiasing the constant global voltages.

IV. TRANSIENT RESPONSE

A. First Topology

The circumstances under which the current mirror will be slowest are when the input current is smallest (in the nA to pA range). In these cases, transistor $M1$ is operating in weak inversion and it is safe to consider the OTA as acting as an instantaneous device which does not introduce any delay. If this is the case, the large signal transient response of the circuit in Fig. 3(b) can be computed by modeling the mirror input stage, as shown in Fig. 4(a), but with $C_{pa} = 0$. If g_{ma}

and g_{oa} model the OTA and $I_{M1} = I_{S1} \exp\{(V_{G1} - v_1)/nU_T\}$ is the current through transistor $M1$, straightforward analysis yields the following state equation:

$$I_{\text{in}} = I_{M1} + \frac{C_p}{g_{oa}A_v}\dot{I}_{M1} + C_p\frac{nU_t}{A_v}\frac{\dot{I}_{M1}}{I_{M1}} \qquad (9)$$

where $A_v = g_{ma}/g_{oa}$ is the OTA voltage gain. If I_{in} changes in a step fashion from rI_c to I_c, the solution for (9) can be written as

$$\frac{I_{M1}(t)}{[I_c - I_{M1}(t)]^{1+\varepsilon}} = \frac{rI_c}{[I_c - rI_c]^{1+\varepsilon}}e^{t/\tau_1} \qquad (10)$$

where

$$\tau_1 = \frac{C_p nU_T}{A_v I_c}, \qquad \varepsilon = \frac{I_c}{g_{oa}nU_T}. \qquad (11)$$

If we define t_{d1} as the delay time it takes for $I_{M1}(t)$ to reach RI_c, then

$$t_{d1} = \tau_1 \ln\left[\frac{R}{r}\left(\frac{1-r}{1-R}\right)^{1+\varepsilon}\right]. \qquad (12)$$

Note that if A_v is sufficiently large, τ_1 can be reasonably small, even for low values of I_c.

As I_c increases, the circuit will respond faster and the delay introduced by the OTA will start to be appreciable. In this case, the circuit shown in Fig. 4(a) with $C_{pa} \neq 0$ can be used to analyze

its transient response. The resulting state equation does not have an analytical solution, thus, in order to obtain an estimation of the delay in the current mirror, one can resort to its small-signal equivalent circuit and consider that I_{in} makes a little step. Neglecting the OTA internal delay[2] (characterized by ω_a) the following characteristics equation (valid for weak and strong inversion) results for the circuit drawn in Fig. 3(c)

$$s^2 + \frac{s}{\tau_3} + \frac{1}{\tau_1 \tau_a} = 0 \quad \begin{cases} \dfrac{1}{\tau_3} = \dfrac{g_{oa} + g_{m1}}{C_{pa}} + \dfrac{g_{o1}}{C_p} \\[2mm] \dfrac{1}{\tau_1} = \dfrac{g_{m1} A_v}{C_p} \\[2mm] \dfrac{1}{\tau_a} = \dfrac{g_{oa}}{C_{pa}}. \end{cases} \quad (13)$$

The roots for this equation are given by

$$s_o = -\frac{1}{2\tau_3}\left[1 \pm \sqrt{1 - 4\frac{\tau_3^2}{\tau_1 \tau_a}}\right]. \quad (14)$$

If $\tau_3^2/\tau_1\tau_a > 1/4$, two complex poles result and the transient has an associated time constant of the order of $2\tau_3$. If the poles are real, the dominant time constant may range from $2\tau_3$ (for high values of $\tau_3^2/\tau_1\tau_a$) to $\tau_1\tau_a/\tau_3$ (for small values of $\tau_3^2/\tau_1\tau_a$). Note that for very small values of I_{in} ($g_{m1} \approx 0$ and $g_{o1} \approx 0$) it follows that $\tau_3^2/\tau_1\tau_a \ll 1$ and $\tau_a \approx \tau_3$, and the resulting time constant is τ_1, as derived previously using the large-signal first-order model. On the other hand, for very large I_{in} (and g_{m1}) values $\tau_3^2/\tau_1\tau_a$ is also small and a dominant first-order dynamics results, with time constant $\tau_1\tau_a/\tau_3 \approx C_p/g_{ma}$. Consequently, for both very small I_{in} and very large I_{in} there are no complex poles and the dynamics are dominated by a single real pole. The maximum value of $\tau_3^2/\tau_1\tau_a$ is reached for $g_{m1} = g_{oa}$ (assuming $g_{m1}/C_{pa} \gg g_{o1}/C_p$) and is $A_v C_{pa}/4C_p$. Therefore, if $A_v < C_p/C_{pa}$ can be satisfied, no complex poles (and no ringing) will appear for the whole input current range.

If a compensation capacitor C_A is used, the resulting equation would be

$$s^2 + \frac{s}{\tau_3'} + \left(\frac{1}{\tau_a'}\right)^2 = 0 \quad (15)$$

where $\tau_3' = a/b$ and $(\tau_a')^2 = a/c$ with a, b, and c given by (7). Again, the associated dominant time constant would take a value between $2\tau_3'$ and $\tau_a'^2/\tau_3'$. For very small and very large I_{in}, there is a dominant real pole of time constant $\tau_a'^2/\tau_3'$ that produces a first-order dynamics. For very small I_{in}, it results $\tau_a'^2/\tau_3' \approx \tau_1 + C_A/g_{m1}$, while for very large I_{in}, it is $\tau_a'^2/\tau_3' \approx C_p/g_{ma}$. The maximum $(2\tau_3'/\tau_a)^2$ value is reached for $g_{m1} \approx g_{oa} + g_{ma}C_A/C_p$, for which two real poles result, both of similar time constants around $1/\tau_3' = 2(g_{oa}/C_A + g_{ma}/C_p)$.

B. Second Topology

For the current mirror of Fig. 3(d) similar analyses can be done. For very small input currents, such that the OTA can be considered to respond instantaneously, the following state equation results (assuming $C_{pa} \approx 0$ and $C_{gs1} \approx 0$)

$$I_{\text{in}} = I_{M1} + \frac{C_p}{g_{oa}(A_v + 1)}\dot{I}_{M1} + \frac{C_p n U_T}{A_v + 1}\frac{\dot{I}_{M1}}{I_{M1}}. \quad (16)$$

Consequently, (10)–(12) would also be valid for this mirror as long as A_v is substituted by $A_v + 1$.

If the OTA is no longer considered to respond instantaneously, or if C_{gs1} is not negligible with respect to C_p, an estimation of the delays

---

[2] The effect of ω_a might be included, although the main delay introduced by the OTA is given by g_{ma} loaded by C_{pa} and other loads.

---

can be obtained from the small-signal equivalent circuit of Fig. 3(d) with $\omega_a = 0$. Routine analysis yields the following characteristics equation (valid for weak and strong inversion):

$$s^2 + \frac{s}{\tau_4} + \frac{1}{\tau_5^2} = 0 \quad \begin{cases} \dfrac{1}{\tau_4} = \dfrac{C_{gs1} + C_p}{C_e^2}g_{oa} + \dfrac{C_{pa} + C_p}{C_e^2}g_{m1} + \dfrac{C_{gs1}}{C_e^2}g_{ma} \\[2mm] \dfrac{1}{\tau_5^2} = \dfrac{g_{ma}g_{m1}}{C_e^2} \\[2mm] C_e^2 = C_p C_{gs1} + C_p C_{pa} + C_{gs1}C_{pa}. \end{cases} \quad (17)$$

Consequently, the settling of the mirror has a dominant time constant that can range between values of the order of $2\tau_4$ and τ_5^2/τ_4. For very small and very large I_{in} values (and assuming $C_p \gg C_{pa}$, C_{gs1}) it follows that $(2\tau_4/\tau_5)^2 \ll 1$ and a dominant first-order dynamics results, with effective time constant τ_5^2/τ_4. For very small I_{in} this time constant is $\tau_1 + C_{gs1}/g_{m1}$, while for very large I_{in} it is C_p/g_{ma}. The maximum value for $(2\tau_4/\tau_5)^2 = (C_{gs1} + C_{pa})/C_{gs1} + C_p/A_v)$ is reached for $g_{m1} = g_{oa} + g_{ma}C_{gs1}/C_p$. Therefore, if $A_v C_{pa} < C_p$ can be satisfied no complex poles will appear.

C. Simulations

Extensive Hspice transient response simulations have been performed on both topology current mirrors to confirm the previous analyses. Sizes for transistors $M1$ and $M2$ were set to 150 μm × 5 μm and the internal bias current for the OTA was 20 μA. An input node capacitance of $C_p = 1$ pF was considered and the input current was changed in a step fashion from I_c to $2I_c$. The value of I_c was swept logarithmically from 10 pA to 10 μA. The output of the current mirror was connected to a voltage source equal to $V_{\text{CLAMP}} = 2.5$ V. The current through this voltage source $I_o(t)$ was time-normalized to $I_o(t/\tau_n)$, where τ_n is the time at which I_o has reached 63.2% of its total excursion value (assuming a first-order-like response). Fig. 5(a) shows the simulated output waveforms, where the amplitude has also been normalized with respect to I_c,

$$\frac{I_o(t/\tau_n) - I_c}{I_c}. \quad (18)$$

In Fig. 5(b), for the trace with circles, the corresponding values for τ_n as a function of I_c are represented for Topology 1 with $C_A = 0$. As discussed previously, in Section IV-A, for very small currents, the time constant is inversely proportional to the current level [see (11)], while for large currents, the time constant tends to settle to a constant value [see discussion after (14)]. For I_c between 2 and 100 nA, the mirror output current step response showed ringing (presence of complex conjugate poles), while outside this range no ringing is observed (absence of complex conjugate poles). This was also predicted by the theoretical discussion after (14). Eventually, ringing could be reduced or suppressed by improving the circuit phase margin by adding the compensation capacitance C_A mentioned in Section III-A. However, C_A may increase the delays for the complete range of input currents.

The same simulations were repeated for the second topology. The resulting values of τ_n as a function of I_c are represented in Fig. 5(b), using the trace with asterisks. Again, for very small currents, the time constant is inversely proportional to current and tends to settle for large currents (as predicted in Section IV-B). Presence of complex conjugate poles was observed for I_c between 10 and 100 nA, as anticipated by the discussion after (17). Note that for the lower current ranges the resulting values for τ_n are about twice than those for Topology 1. This is because for Topology 2 the input node capacitance C_p also now includes the subthreshold gate-to-bulk C_{gb} capacitance of transistor $M1$. For gate oxide thickness

(a)   (b)
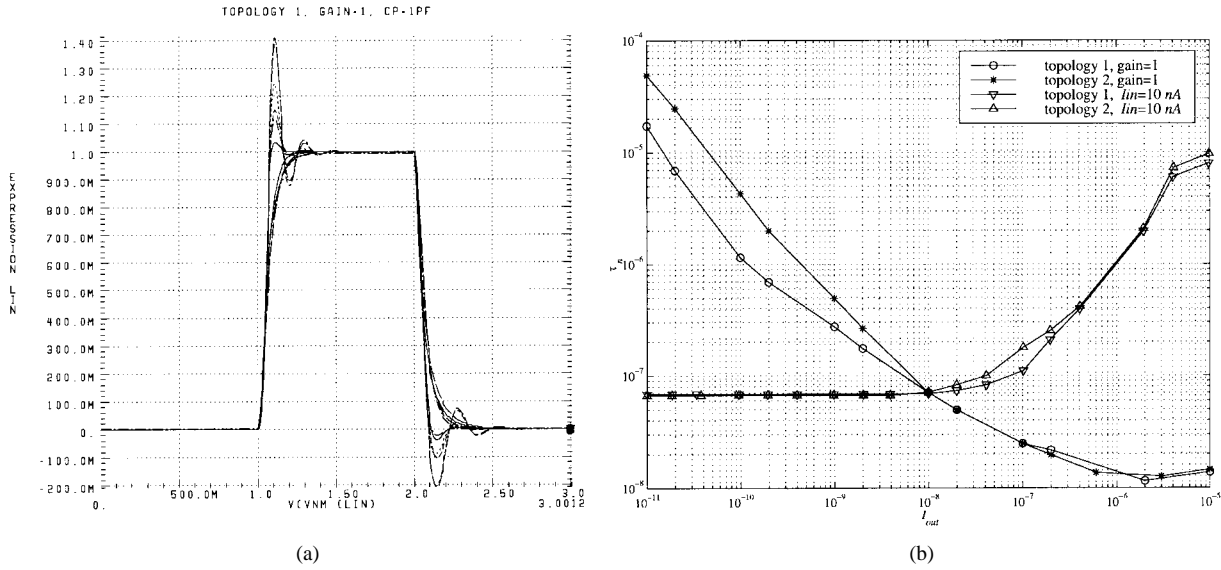
Fig. 5. Transient analyses simulation results. (a) Time and amplitude normalized transient responses for Topology 1 current mirror with unity gain. (b) Extracted values for τ_n for both topologies with unity gain and sweeping the gain.

(a)   (b)   (c)
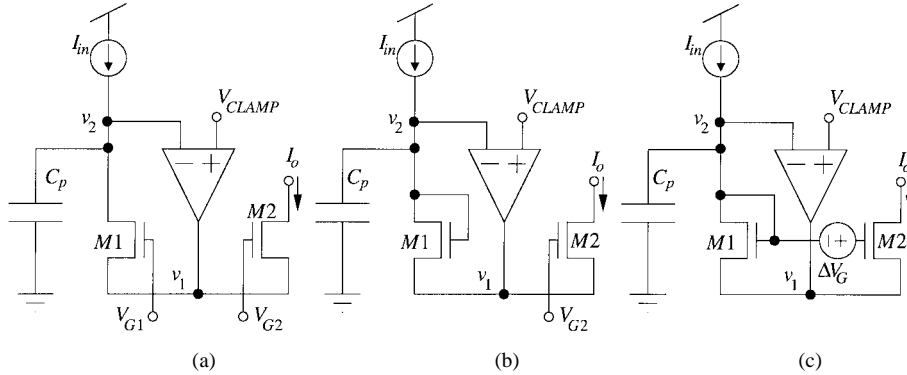
Fig. 6. Continuously adjustable gain current mirror versions. (a) First new topology. (b) Second topology with absolute gate bias. (c) Relative gate bias.

$t_{ox} = 10$ nm and gate area $A = 150 \times 5 \ \mu\text{m}^2$ this capacitance is $C_{gb} = 0.44 \ A\varepsilon_{ox}/t_{ox} = 1.05$ pF [8]. Therefore, in this example the effective C_p capacitance is about twice than for Topology 1, for the lower current range, which precisely explains the different τ_n values.

V. CONTINUOUSLY ADJUSTABLE GAIN

The functionality of these current mirrors can be further extended when they operate in weak inversion. The current mirrors gain can be made continuously adjustable through a control voltage, and the adjustment range can be very wide (over 11 decades, as shown later in the section on experimental results). The way this is achieved is very simple. By connecting the gate of transistor $M2$ to an independent bias voltage V_{G2}, the gain of the current mirrors can be continuously controlled through voltage V_{G2}. This is shown in Fig. 6 for the two proposed current mirrors. Under these circumstances, the currents through transistors $M1$ and $M2$ are given by

$$
\begin{aligned}
I_{\text{in}} &= I_{s1}e^{(V_G - v_1)/nU_T} \\
I_o &= I_{s2}e^{(V_{G2} - v_1)/nU_T}
\end{aligned}
\tag{19}
$$

where U_T is the thermal voltage, V_G is the gate voltage of transistor $M1$ [$V_G = V_{G1}$ for Fig. 6(a), and[3] $V_G = V_{\text{CLAMP}}$ for Fig. 6(b) and

[3] Strictly speaking, for Fig. 6(b) $V_G = V_{\text{CLAMP}} + V_{\text{off}} + [I_{\text{in}}/g_{oa} + \ln(I_{\text{in}}/I_{s1})]/(A_v + 1)$ where V_{off} is the input offset voltage of the OTA.

(c)], and I_{s1} and I_{s2} are positive parameters which can be considered to be equal if transistors $M1$ and $M2$ are of equal size and properly well matched. From (19) the current mirror output current is

$$
I_o = A_i I_{\text{in}}
\tag{20}
$$

where A_i, which is a function of $V_{G2} - V_G$, is the gain of the current mirror and is equal to

$$
A_i = \frac{I_{s2}}{I_{s1}} e^{(V_{G2} - V_G)/nU_T}.
\tag{21}
$$

Since $V_{G2} - V_G$ controls exponentially the current mirror gain, a very wide tuning range is expected.

If there is a mismatch between transistors $M1$ and $M2$, it will influence (21) through parameters I_{s1} and I_{s2}. Statistically, the standard quadratic relative deviation of the gain is given by

$$
\sigma^2(\Delta A_i/A_i) = \sigma^2(\Delta I_{s1}/I_{s1}) + \sigma^2(\Delta I_{s2}/I_{s2}) + \frac{\sigma^2(V_{\text{off}})}{V_{EA}^2}
\tag{22}
$$

where V_{EA} is transistors' $M1$ and $M2$ early voltage and V_{off} is the OTA offset voltage. Note that (22) is independent of the value of V_{G2} and V_G. For the mirror of Fig. 6(b), the offset introduced by the OTA changes (22) to

$$
\sigma^2(\Delta A_i/A_i) = \sigma^2(\Delta I_{s1}/I_{s1}) + \sigma^2(\Delta I_{s2}/I_{s2}) + \frac{\sigma^2(V_{\text{off}})}{n^2 U_T^2}
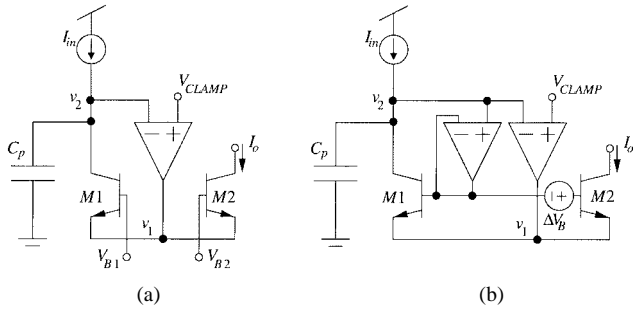\tag{23}
$$

Fig. 7. Bipolar versions of continuously adjustable gain current mirrors. (a) First topology. (b) Second topology.

where the $V_{\rm off}$ contribution term is much larger, which might render the circuit unacceptable. In this case, the mirror gain should be adjusted by controlling the differential voltage between the gates of transistors $M1$ and $M2$, as shown in Fig. 6(c). In this case, (22) is valid again.

The relative noise spectral density at the output current I_o is given for Fig. 6(a) and (c) by

$$\frac{\overline{i_o^2}}{I_o^2} = \frac{1 + \left(\dfrac{\omega}{\omega_2}\right)^2}{1 + \left(\dfrac{\omega}{\omega_1}\right)^2} \frac{\overline{i_{n1}^2}}{I_{\rm in}^2} + \frac{1 + \left(\dfrac{\omega}{\omega_3}\right)^2}{1 + \left(\dfrac{\omega}{\omega_1}\right)^2} \frac{\overline{i_{n2}^2}}{I_o^2}$$
$$+ \frac{1 + \left(\dfrac{\omega}{\omega_4}\right)^2}{1 + \left(\dfrac{\omega}{\omega_1}\right)^2} \frac{\overline{v_{na}^2}}{V_{EA}^2} \qquad (24)$$

where $\overline{i_{n1}}$ and $\overline{i_{n2}}$ are the noise spectral density currents generated by $M1$ and $M2$, respectively, $\overline{v_{na}}$ is the equivalent input noise spectral density for the OTA, and

$$\omega_1^{-1} = C_p \left(\frac{1 + A_i}{g_{ma}} + \frac{1}{g_{m1} A_v} \right)$$
$$\omega_2^{-1} = \frac{C_p}{g_{ma}}$$
$$\omega_3^{-1} = C_p \left(\frac{1}{g_{ma}} + \frac{1}{g_{m1} A_v} \right)$$
$$\omega_4^{-1} = \frac{C_p}{g_{o1}} \qquad (25)$$

with $A_v = g_{ma}/g_{oa}$ being the OTA voltage gain. Note that, by (24), the output noise is not degraded by the fact that A_i might become extremely large or extremely small. For Fig. 6(b) the output current relative noise spectral density is given by

$$\frac{\overline{i_o^2}}{I_o^2} = \frac{1 + \left(\dfrac{\omega}{\omega_2}\right)^2}{1 + \left(\dfrac{\omega}{\omega_1}\right)^2} \frac{\overline{i_{n1}^2}}{I_{\rm in}^2} + \frac{1 + \left(\dfrac{\omega}{\omega_3}\right)^2}{1 + \left(\dfrac{\omega}{\omega_1}\right)^2} \frac{\overline{i_{n2}^2}}{I_o^2}$$
$$+ \frac{1 + \left(\dfrac{\omega}{\omega_5}\right)^2}{1 + \left(\dfrac{\omega}{\omega_1}\right)^2} \frac{\overline{v_{na}^2}}{n^2 U_T^2} \qquad (26)$$

with $\omega_5^{-1} = C_p/g_{m1}$. Note that the OTA noise contribution here is significantly larger than in (24), which might render this topology useless.
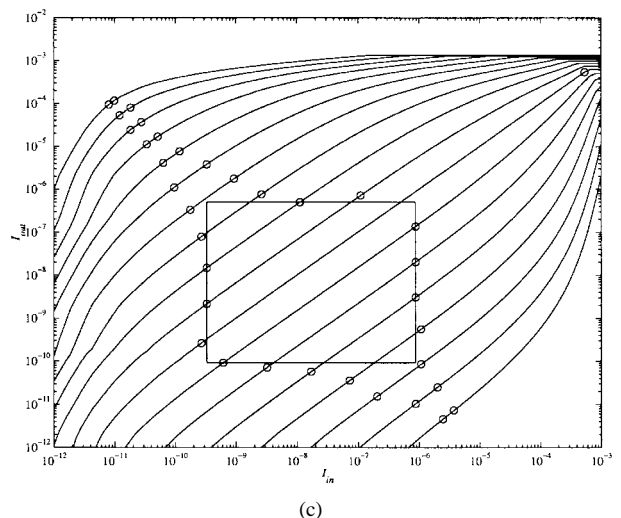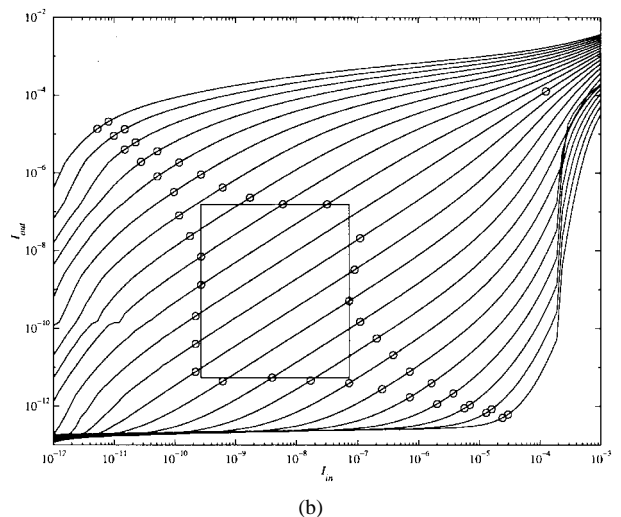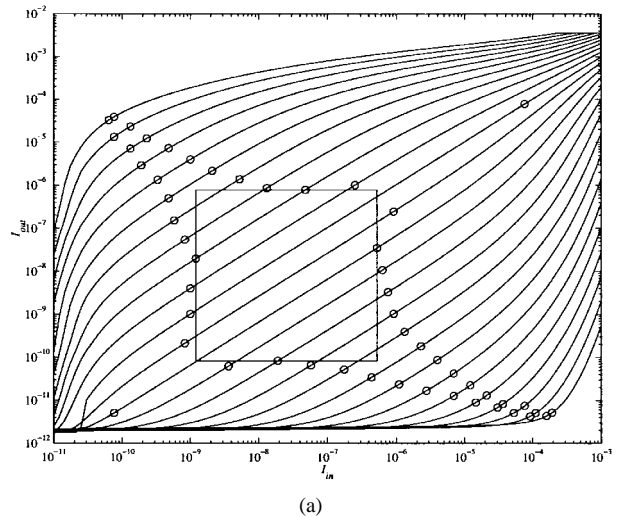

(a)

(b)

(c)

Fig. 8. Experimentally measured output versus input currents, for different gains. (a) The NMOS mirror. (b) The PMOS mirror. (c) The bipolar mirror versions.

VI. LOADING EFFECTS

The stability analyses developed in Section III are based on the assumption that stability behavior of the circuit in Fig. 3(a) can be analyzed by using the circuit in Fig. 3(b). However, this is true if the

TABLE I
1% LINEARITY ERROR REGIONS

	Absolute		Unity Gain	
	A_{min}	A_{max}	I_{min}	I_{max}
NMOS	6.1×10^{-7}	1.8×10^{5}	1.0×10^{-9}	7.7×10^{-5}
PMOS	5.7×10^{-7}	2.6×10^{6}	2.1×10^{-10}	1.2×10^{-4}
Bipolar	1.9×10^{-6}	4.5×10^{6}	2.7×10^{-10}	5.4×10^{-4}

TABLE II
1% ERROR BOX REGIONS

	I_{in}^{min}	I_{in}^{max}	I_{out}^{min}	I_{out}^{max}	A_{min}	A_{max}
NMOS	1.2 nA	520 nA	83 pA	780 nA	2.9×10^{-4}	2.7×10^{2}
PMOS	0.27 nA	72 nA	5.4 pA	160 nA	2.7×10^{-4}	1.4×10^{2}
Bipolar	0.33 nA	871 nA	92 pA	500 nA	5.1×10^{-4}	3.0×10^{2}

Fig. 9. Constant linear input range OTA using the Topology-1 current mirror.

current flowing through transistor $M2$ does not alter the stability conditions derived by using the circuit in Fig. 3(b). Note that if current mirror gain adjustment is used (as in Fig. 6), the current through transistor $M2$ can be several orders of magnitude larger than the one through transistor $M1$. Furthermore, the load connected at the drain of transistor $M2$ is going to be coupled to the current mirror circuitry through the output conductance of $M2$. On the other hand, since the gate of $M2$ is connected to a fixed voltage, no capacitive coupling (through C_{dg2} and/or C_{gs2}) exists between the load and the current mirror circuitry. Assuming the load at the drain of transistor $M2$ can be approximated by the parallel connection of a resistance and a capacitance, small-signal analysis reveals that the stability conditions for both topologies are relaxed. Consequently, the conditions developed in Section III are more stringent and are the ones to be used.

The transient response analyses in Section IV neglect completely the loading effect of transistor $M2$. Strictly speaking, this is only true if, for equal size $M1$ and $M2$ transistors, the gain of the mirror is much less than unity, so that the current through $M2$ is negligible with respect to the one through $M1$. However, if the gain is unity or larger, a slower response is expected because the OTA has to provide a significantly larger current.

For Topology 1, very small currents and neglecting the loads at the drain of $M2$, it is easy to show that (9) changes to

$$I_{\text{in}} = I_{M1} + \frac{C_p(1 + A_i)}{g_{oa}A_v} \dot{I}_{M1} + C_p \frac{nU_T}{A_v} \frac{\dot{I}_{M1}}{I_{M1}} \qquad (27)$$

where A_i is the gain of the current mirror. This implies that (10)–(12) remain valid as long as ε is substituted by

$$\varepsilon' = (1 + A_i)\varepsilon \qquad (28)$$

which reveals that delay t_{d1} in (12) is degraded, at the most, by a factor of A_i. If capacitance C_{pa} cannot be neglected and/or $C_A \neq 0$, small-signal analysis can be performed to estimate the time constant degradation. For high current amplification values A_i it can be verified that the resulting time constant is degraded, at the most, by a factor of the order of A_i.

Hspice simulations were performed using the same circuit as in Section IV-C, Topology 1, but with a constant input current step from $I_c = 10$ nA to $2I_c = 20$ nA and sweeping the mirror gain from $A_i = 10^{-3}$ to $A_i = 10^{+3}$. The results are shown in Fig. 5(b)
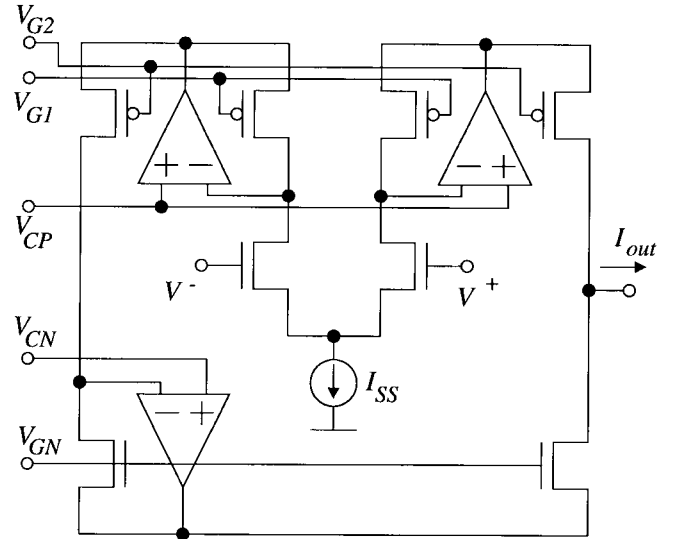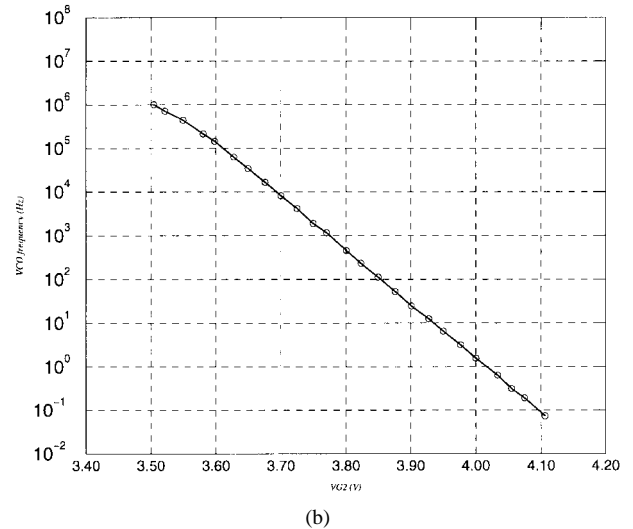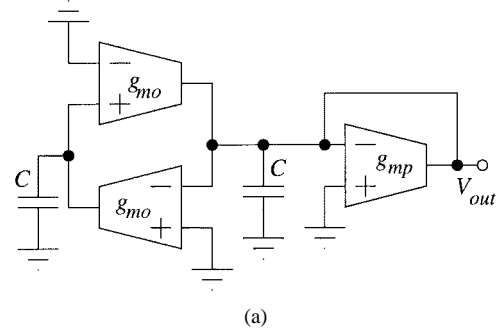

(a)

(b)

Fig. 10. (a) Sinusoidal g_m-C based VCO. (b) Experimentally measured relationship between sinusoidal VCO frequency and control voltage V_{G2}.

using the trace with down triangles. For gains smaller than unity, time response is constant, while for gains larger than unity, the time response is degraded as A_i increases. As can be seen, the resulting time constant is increased, at the most, by a factor A_i.

For Topology 2 and very small currents a much more complicated differential equation than (24) is obtained, which does not have an analytical solution. However, by performing Hspice simulations on this topology with $I_c = 10$ nA, shown in Fig. 5(b) with up triangles,

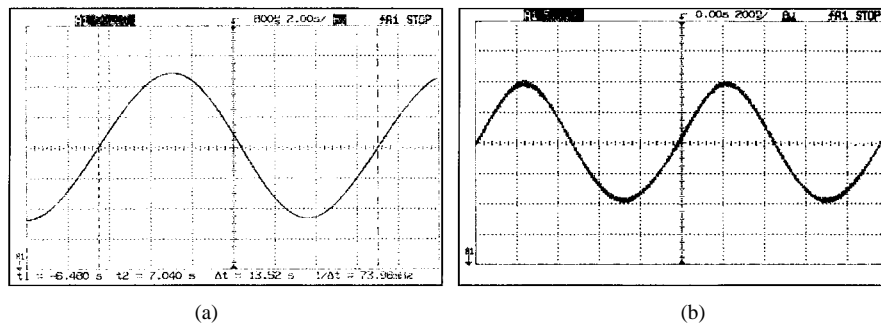(a)   (b)

Fig. 11.   Measured VCO outputs for minimum (73.94 mHz) and maximum (1.015 MHz) frequencies. Vertical scale is 50 mV/div and horizontal scales are 2 s/div for left trace and 200 ns/div for right trace.
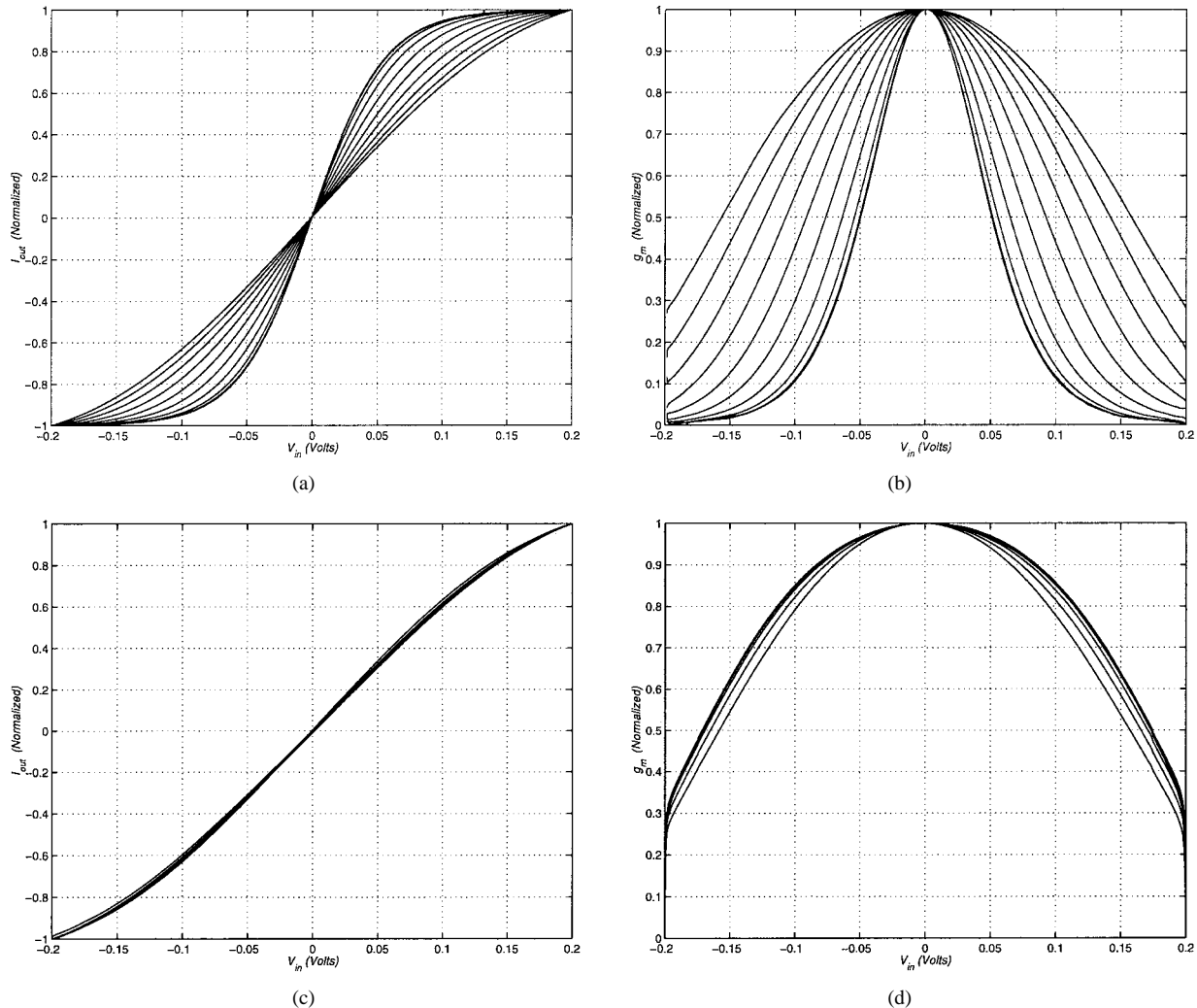

(a)   (b)

(c)   (d)

Fig. 12.   Experimentally measured dependence of the OTA linear input range on transconductance tuning. For differential pair tail bias current (I_{SS}) tuning, linear range decreases as transconductance decreases. (a) Normalized OTA output current (I_{out}/I_{SS}) as a function of differential input voltage. (b) Normalized first derivative of previous curve. For tuning through the top Topology-1 current mirrors. (c) Normalized OTA output current. (d) Normalized first derivative of previous curve.

it is observed that the time constant degradation is similar to that for Topology 1. Again, for high A_i values, time constants are degraded, at the most, by a factor of the order of A_i.

VII. CMOS COMPATIBLE LATERAL BIPOLAR MODE

The two new current mirror topologies discussed so far can also be operated by biasing the transistors as CMOS compatible lateral bipolars [8]. The circuits in Figs. 3 and 6 can be biased to operate transistors $M1$ and $M2$ as lateral bipolars if the process is p well. For an n well process, p-type current mirrors are the ones that can be biased in the lateral bipolar mode. The first topology [Fig. 6(a)] can be used directly by rebiasing the gate and well voltages, while the second topology requires the use of an extra differential voltage amplifier or OTA. Fig. 7(a) shows the bipolar version of the current mirror in Fig. 6(a). Physically both circuits are the same. The difference is

how the gates and wells of transistors $M1$ and $M2$ are biased. In Fig. 6(a), the wells are connected to ground (or to positive power supply for a PMOS mirror), while V_{G1} and V_{G2} should be connected to intermediate voltage values such that, for the current levels used, the OTA output voltage does not saturate. In Fig. 7(a) both gates must be connected about 1 V below ground (or above positive power supply for the p version) [8] and the wells, which are now the base terminals, to intermediate values. For the bipolar version of the second topology, an extra OTA must be added to decouple the nonzero base currents. The resulting circuit is shown in Fig. 7(b).

VIII. EXPERIMENTAL RESULTS

A set of current mirror prototypes have been fabricated in a 1.2-μm n-well CMOS process. Transistors were laid out as square waffle structures with $L = 4.8$ μm and effective $W = 1378$ μm. In this case, an OTA able to provide several milliamps of output current was used. Fig. 8 shows measurements of I_o versus I_{in}, for different gains, for an NMOS, a PMOS, and a lateral bipolar p-n-p mirror, corresponding to the topologies of Figs. 6(a) and 7(a). In Fig. 8, input currents were swept between 1 pA and 1 mA. Gain control voltage (V_{G2} or V_{B2}) was swept with 50 mV steps around V_{G1} or V_{B1}. In these log–log representations, lines of slope one represent a linear relationship between input and output currents, while line position accounts for the gain. Circles denote the 1% linearity error region limits. For these regions, the maximum and minimum current mirror gains are given in Table I as A_{min} and A_{max}. Also shown in Fig. 8 are the maximum size rectangles that could be drawn inside the 1% linearity error regions. Maximum and minimum currents and gains for these boxes are given in Table II. Note that in Fig. 8, for the unity gain curves, the 1% error interval is significantly larger than for the other curves. These limits are given in Table I under I_{min} and I_{max}.

As an application example, the Topology-1 current mirror was used to design the OTA shown in Fig. 9, which is used in the g_m-C sinusoidal VCO shown in Fig. 10 [6]. The oscillation frequency for this VCO is given by

$$f_{VCO} = \frac{1}{2\pi} \frac{g_{mo}}{C}. \tag{29}$$

For the fabricated prototype VCO, the capacitor value is $C = 10$ pF. When using conventional CMOS OTA's for g_m-C sinusoidal VCO's, their frequency tuning range is limited to little more than one decade [6]. The reason is that for tuning the VCO frequency, OTA transconductances must be changed. If the OTA transconductance is adjusted through its differential pair bias current I_{ss}, then the linear range of the OTA is reduced as its transconductance (and I_{ss}) is lowered. If a linear range above 200 mV is desired, transconductance tuning is limited to little more than one decade. The transconductance of the OTA in Fig. 9 can be tuned while maintaining its I_{ss} current (and linear range) constant. The two top Topology-1 PMOS current mirrors are tuned simultaneously through control voltage V_{G2} and are able to change the OTA transconductance for over seven decades. Fig. 10(b) shows the experimentally obtained relationship between oscillation frequency and control voltage V_{G2} of the sinusoidal VCO. The minimum frequency that could be measured was $f_{min} = 73.96$ mHz, while the maximum was $f_{max} = 1.015$ MHz. Fig. 11 shows the measured sinusoidal waveforms for these two limit situations.

To show the effect of OTA linear input range degradation, let us resort to Fig. 12. Classically, the OTA transconductance g_m is tuned by changing its differential pair tail bias current I_{SS}. Fig. 12(a) shows the measured curves $I_{out}(V_{in})/I_{SS}$ for the OTA of Fig. 9 ($V_{in} = V^+ - V^-$) when using current I_{SS} for tuning and leaving V_{G2} constant. Fig. 12(b) shows the curves $I'_{out}(V_{in})/g_m$, which are

the first derivatives of those in Fig. 12(a) normalized with respect to g_m [defined as the slopes at $V_{in} = 0$ for Fig. 12(a)]. The widest bell-shaped curve corresponds to the maximum I_{SS} and maximum g_m. As I_{SS} is decreased, the bells become narrower (lower input range) until the differential pair transistors are fully biased in weak inversion and the linear input range remains constant (between one or two nU_T). In Fig. 12(a) and (b) the largest measured transconductance is $g_m = 30.0$ μA/V, while the minimum is $g_m = 60.4$ pA/V. If, instead of using I_{SS} to tune g_m we use V_{G2}, then the curves shown in Fig. 12(c) and (d) are measured. Fig. 12(c) shows $I_{out}(V_{in})/|I_{out}^{max}|$ and Fig. 12(d) shows $I'_{out}(V_{in})/g_m$. In Fig. 12(c) and (d), the largest measured transconductance is $g_m = 30.0$ μA/V, while the minimum is $g_m = 40.0$ pA/V. Note that now the OTA input range is maintained constant. As a result, the OTA behaves almost linearly from -100 mV to $+100$ mV, which means that low distortion sinusoids of 200 mV peak-to-peak amplitude can be obtained with the VCO of Fig. 10 for the whole frequency range, as can be seen in Fig. 11.

IX. CONCLUSIONS

Two new active-input current mirror structures are introduced. The novelty resides in the fact that the active amplifier drives the transistor sources rather than the gates. This allows the amplifier to be connected in a negative feedback loop configuration, instead of a positive feedback loop. The first proposed topology might require compensation, while the second does not. Both topologies behave much better from a stability point of view than the conventional active-input current mirror. This is because the amplifier output is connected to a low-impedance node. The result is that the mirrors remain stable for arbitrarily small operation currents, thus allowing current ranges of many decades. Experimental measurements reveal that the currents involved can vary over nine decades and that the gain of these current mirrors can be continuously tuned over 11 decades, while maintaining a 1% linearity error in the mirroring operation. The mirrors can be used either with their transistors biased as MOS, or as CMOS compatible lateral bipolar devices. Experimental results have been provided. As an application example, a g_m-C sinusoidal VCO has been fabricated and tested. Its frequency could be continuously tuned for over seven decades, through a single control voltage.

REFERENCES

[1] C. Mead, *Analog VLSI and Neural Systems.* Reading, MA: Addison-Wesley, 1989.

[2] A. G. Andreou, R. C. Meitzler, K. Strohbehn, and K. A. Boahen, "Analog VLSI neuromorphic image acquisition and pre-processing systems," *Neural Networks,* vol. 8, nos. 7/8, pp. 1323–1347, 1995.

[3] D. G. Nairn and A. T. Salama, "A ratio-independent algorithmic analog-to-digital converter combining current mode and dynamic techniques," *IEEE Trans. Circuits Syst.,* vol. 37, pp. 319–325, Mar. 1990.

[4] T. Serrano and B. Linares-Barranco, "The active-input regulated-cascode current mirror," *IEEE Trans. Circuits Syst. I,* vol. 41, pp. 464–467, June 1994.

[5] P. E. Allen and D. R. Holberg, *CMOS Analog Design.* New York: Holt, Rinehart and Winston, 1987.

[6] B. Linares-Barranco, A. Rodríguez-Vázquez, J. L. Huertas, and E. Sánchez-Sinencio, "On the generation design and tuning of OTA-C high frequency sinusoidal oscillators," *IEE Proc. Pt. G* vol. 139, no. 5, pp. 557–568, Oct. 1992.

[7] M. G. Degrauwe, J. Rijmenants, E. A. Vittoz, and H. J. De Man, "Adaptive biasing CMOS amplifiers," *IEEE J. Solid-State Circuits,* vol. SC-17, pp. 522–528, June 1982.

[8] Y. P. Tsividis, *Operation and Modeling of the MOS Transistor.* New York: McGraw-Hill, 1987.

[9] X. Arreguit, "CMOS compatible bipolar lateral transistor," Ph.D. dissertation, EPFL, Lausanne, Switzerland, 1985.